

DGS-Net: Distillation-Guided Gradient Surgery for CLIP Fine-Tuning in AI-Generated Image Detection

Jiazhen Yan¹, Ziqiang Li¹, Fan Wang², Boyu Wang¹, Zhangjie Fu^{1*}

¹ School of Computer Science, Nanjing University of Information Science and Technology

² University of Macau

247918horizon@gmail.com, iceli@mail.ustc.edu.cn, wf71103@126.com, fzj@nuist.edu.cn

Abstract

The rapid progress of generative models such as GANs and diffusion models has led to the widespread proliferation of AI-generated images, raising concerns about misinformation, privacy violations, and trust erosion in digital media. Although large-scale multimodal models like CLIP offer strong transferable representations for detecting synthetic content, fine-tuning them often induces catastrophic forgetting, which degrades pre-trained priors and limits cross-domain generalization. To address this issue, we propose the Distillation-guided Gradient Surgery Network (DGS-Net), a novel framework that preserves transferable pre-trained priors while suppressing task-irrelevant components. Specifically, we introduce a gradient-space decomposition that separates harmful and beneficial descent directions during optimization. By projecting task gradients onto the orthogonal complement of harmful directions and aligning with beneficial ones distilled from a frozen CLIP encoder, DGS-Net achieves unified optimization of prior preservation and irrelevant suppression. Extensive experiments on 50 generative models demonstrate that our method outperforms state-of-the-art approaches by an average margin of 6.6%, achieving superior detection performance and generalization across diverse generation techniques.

1. Introduction

The rapid advancement of deep learning has driven significant progress in generative models such as generative adversarial networks (GANs) [28, 33, 57] and diffusion models [25, 63, 84]. Owing to their low generation cost and high visual fidelity, these models have been widely applied across various domains, including digital art, entertainment, and content creation. However, their widespread use has also raised serious concerns about privacy violations, misinformation dissemination, and the erosion of trust in digital media.

As a result, developing reliable detectors to verify the authenticity of AI-generated images has become an urgent and critical task. Despite notable progress in recent detection approaches [41, 68, 82, 97], achieving robust generalization to unseen generative techniques remains a fundamental and unsolved challenge.

Large-scale multimodal pre-trained models, such as CLIP [60], have recently emerged as powerful tools for detecting AI-generated images. By leveraging transferable representations learned from massive image–text datasets, CLIP constructs a semantic embedding space with strong open-set scalability and cross-domain generalization [70, 89], providing a robust foundation for identifying synthetic images [38, 55, 96] produced by diverse generative models. However, CLIP’s pre-training objective is not explicitly optimized to capture generation artifacts—key cues for distinguishing authentic and synthetic content. To address this limitation, recent studies have adapted CLIP for detection tasks through either full fine-tuning or parameter-efficient tuning strategies [20, 48, 70] such as LoRA [26]. Despite these efforts, fine-tuning often induces **catastrophic forgetting**, eroding the transferable priors and geometric structure of the pre-trained embedding space. Consequently, the adapted model may overfit to dataset-specific patterns rather than learning artifact-level features that generalize across different generative mechanisms.

To investigate this phenomenon, we construct four datasets using ProGAN [33], R3GAN [28], SDXL [59], and SimSwap [9], each containing both real and generated images across multiple categories. We then extract features using three variants of CLIP: the original pre-trained model [55], a LoRA fine-tuned model, and our proposed method. The extracted features are visualized using t-SNE, as shown in Figure 1. The frozen CLIP model preserves the geometric structure and local coherence learned during pre-training but exhibits weak real/fake separability. In contrast, LoRA fine-tuning enhances separability but collapses the representation geometry and degrades cross-domain detection performance.

*Corresponding author

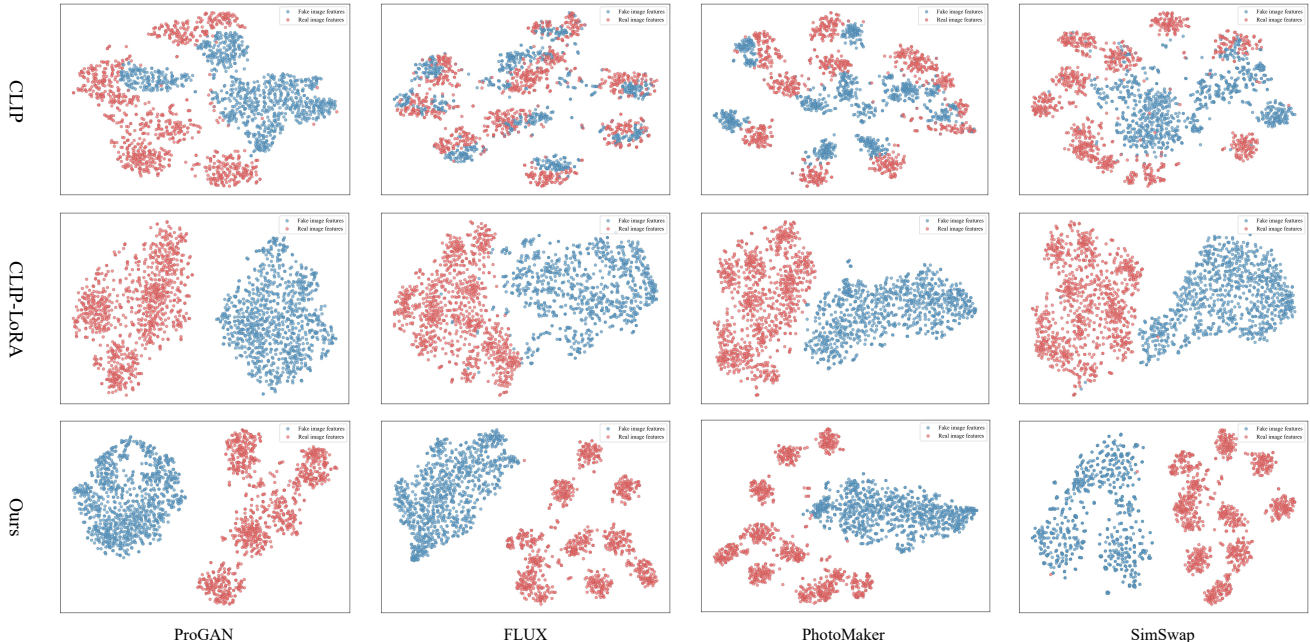


Figure 1. **T-SNE Visualization of Features Extracted Using CLIP, CLIP-LoRA and Ours.** Our method achieves strong real/fake discrimination while simultaneously preserving the prior knowledge embedded in the pre-trained model.

These observations indicate that catastrophic forgetting in existing fine-tuning strategies compromises the transferable priors of the pre-trained model.

To address these issues, we introduce a knowledge distillation framework [24] tailored for CLIP-based detectors. As illustrated in Figure 1, the pre-trained CLIP features inherently contain numerous components unrelated to generation artifacts. Conventional feature distillation methods, which enforce global alignment between teacher and student representations, may inadvertently retain these task-irrelevant factors. Therefore, our goal is to **preserve transferable pre-trained priors** while **suppressing task-irrelevant components**. Specifically, we introduce a gradient-space decomposition strategy, where the positive half-space of task gradients is defined as harmful directions and the negative half-space as beneficial directions (see Sec. 3 for details). Building on this principle, we propose a **Distillation-guided Gradient Surgery Network (DGS-Net)**. During backpropagation, we first project the image gradients of the training network onto the orthogonal complement of the harmful directions estimated from text gradients, effectively suppressing components irrelevant to the detection task. Meanwhile, we exploit the beneficial descent directions extracted from a frozen CLIP image encoder to guide lightweight alignment of the training network’s representations, thereby preserving the transferable priors acquired during pre-training. As shown in Figure 1, our approach achieves strong real/fake discrimination while maintaining the pre-trained model’s

prior knowledge, ultimately enhancing generalization across diverse generative models.

In summary, our work makes following key contributions:

- To the best of our knowledge, this is the first study to systematically diagnose catastrophic forgetting induced by CLIP fine-tuning in AI-generated image detection. We further introduce a novel gradient-space decomposition that disentangles CLIP representations into transferable pre-trained priors and task-irrelevant components.
- We propose an innovative detection framework, **DGS-Net**, which employs distillation-guided gradient decoupling and alignment to preserve transferable pre-trained priors while suppressing task-irrelevant knowledge, thereby improving both detection accuracy and cross-domain generalization.
- Extensive experiments across 50 diverse generative models demonstrate that our method consistently outperforms state-of-the-art approaches, achieving an average improvement of 6.6% in detection accuracy, highlighting its robustness and universality.

2. Related Works

2.1. AI-Generated Image Detection

With the rapid advancement of generative models such as GANs [28, 33, 35, 65] and diffusion models [17, 25, 46, 84], the visual quality of synthetic images has improved dramatically, making it increasingly difficult for the human eye to distinguish real images from generated ones. In response

to the potential misuse of these generative techniques, extensive research has been devoted to AI-generated image detection, which can be broadly categorized into **artifact-based methods** [67, 71, 87, 98] and **data-centric methods** [5, 10, 77]. Artifact-based approaches typically exploit low-level forensic cues that expose generation traces, such as frequency irregularities [51, 68, 86], pixel-level inconsistencies [2, 4, 12], gradient patterns [67], neighboring-pixel dependencies [69], and reconstruction errors [3, 10, 14, 79]. For example, BiHPF [29] enhances artifact visibility by applying dual high-pass filters; LGrad [67] leverages gradients from pretrained CNNs to reveal universal forgery traces; NPR [69] reinterprets upsampling operations to construct an efficient artifact representation; and DIRE [79] captures generation discrepancies via reconstruction error analysis. In contrast, data-centric methods aim to learn more generalizable artifact representations through large-scale data and augmentation strategies. Representative efforts include data augmentation [42, 77] and dataset construction [5, 10, 22, 93]. CNN-Spot [77] enhances model robustness by combining diverse augmentation techniques with large-scale GAN-generated datasets. SAFE [42] integrates cropping and augmentations such as ColorJitter, RandomRotation, and RandomMask to improve generalization. DRCT [5] leverages diffusion-based reconstruction to achieve better semantic alignment, while B-Free [22] mitigates dataset bias using self-conditioned inpainted reconstructions and content-aware augmentation.

With the rapid rise of large pre-trained models, particularly vision-language models such as CLIP [60], recent studies have begun exploiting their powerful feature extraction and semantic understanding capabilities for AI-generated image detection. The impressive generalization ability of CLIP demonstrated in UnivFD [55] has inspired a series of follow-up works that adapt or fine-tune CLIP for improved detection performance. Existing approaches can be broadly divided into two categories: (1) **feature-based methods**, which freeze the pre-trained network and optimize only the extracted features to enhance generalization [38, 55, 96]; and (2) **fine-tuning-based methods**, which update model parameters to learn task-specific features through full fine-tuning, low-rank adaptation (LoRA) [50, 70, 87], or lightweight adaptation modules [48, 71, 89]. For instance, D³ [91] utilizes CLIP as a powerful feature backbone and introduces a parallel branch to disentangle universal fake artifacts from multi-generator images. VIB-Net [96] applies a Variational Information Bottleneck to decouple and filter CLIP-extracted features, effectively suppressing task-irrelevant information. C2P-CLIP [70] injects category-consistent cues into the text encoder and employs contrastive learning to improve cross-modal alignment. Effort [89] constructs two orthogonal subspaces to preserve pre-trained priors while learning forgery-related representations. NS-Net [87] further constructs a NULL-Space of semantic features to remove semantic inter-

ference embedded in visual features.

Despite these advances, existing fine-tuning strategies often degrade the transferable priors of pre-trained models, leading the network to rely on dataset-specific shortcuts rather than learning intrinsic artifact-level cues that generalize across different generators.

2.2. Knowledge Distillation

Knowledge Distillation [24] is a powerful technique for transferring knowledge from a large teacher model to a smaller student model. Numerous studies [15, 30, 43, 78] focus on selecting the most valuable features for knowledge distillation in downstream tasks, with the goal of preserving the richest prior knowledge. This technique has been successfully applied across a variety of domains, including visual recognition [23, 27, 36, 44, 45], language model compression [31, 56, 83], and multimodal representation learning [7, 11, 19]. A seminal work [6] introduced the first distillation framework for object detection, combining feature imitation with prediction mimicking. [58] incorporated a distillation loss into adapter-based fine-tuning to transfer representations from pre-trained models, preventing feature drift during adaptation. [80] proposed feature-level knowledge distillation during fine-tuning, which helps the student model maintain cross-modal semantic alignment while learning downstream tasks.

However, our research shows that not all pre-trained knowledge is beneficial for downstream adaptation, as some representations can negatively impact task performance. In response, we extend the traditional distillation paradigm to selectively retain useful priors while suppressing irrelevant, harmful representations. Unlike conventional feature distillation methods [8, 53, 74, 90], which penalize discrepancies at the representation level, our approach operates in the gradient space. It suppresses gradients that are irrelevant to the task while injecting a small, beneficial knowledge prior into the descent direction, ultimately enhancing the performance of AI-generated image detection.

3. Preliminaries

Before introducing our method, we first establish a directional convention for interpreting the gradient dynamics of classification losses. For any differentiable classification loss, the first-order gradient of the representation indicates the direction of the steepest local variation in the loss landscape [37]. Specifically, a positive gradient value at a given coordinate implies that a positive perturbation along that direction increases the loss (i.e., a **harmful direction**), whereas a negative gradient value implies that a positive perturbation decreases the loss (i.e., a **beneficial direction**).

Formally, let the representation vector be denoted as $u \in \mathbb{R}^d$, and consider a binary classification loss function (e.g., BCEWithLogits) represented by $\mathcal{L}(u, y)$, where

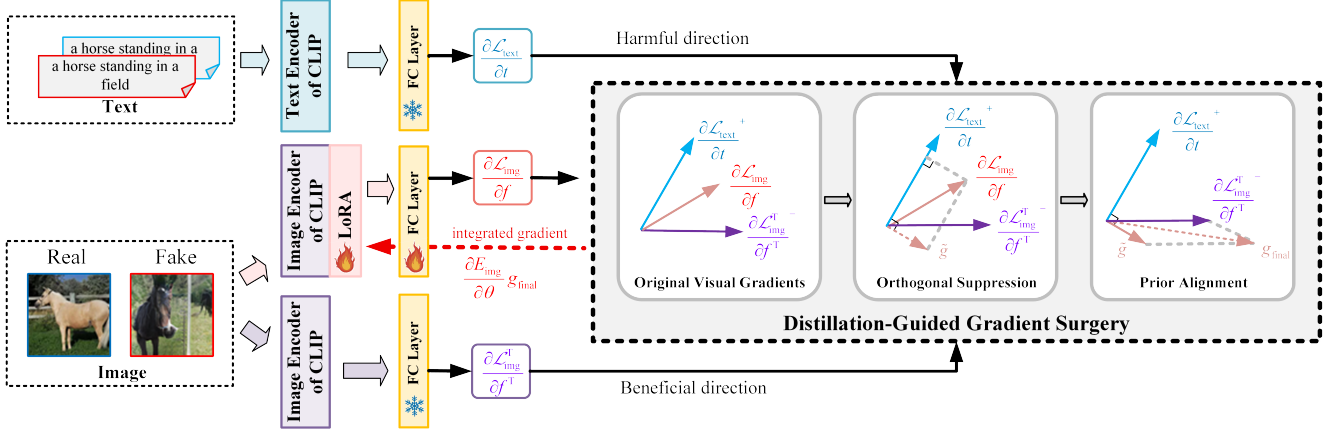


Figure 2. **Overview of the proposed Distillation-guided Gradient Surgery Network (DGS-Net).** We introduce a gradient-space decomposition that separates harmful and beneficial descent directions during optimization. What’s more, it consists of two core components: Orthogonal Suppression and Prior Alignment, which aim to suppress task-irrelevant representations and preserve transferable priors established during large-scale pre-training, substantially enhancing the generalization performance of AI-generated image detection.

$y \in \{0, 1\}$. For any smooth classification loss, the gradient $\nabla_u \mathcal{L}$ indicates the steepest ascent direction of \mathcal{L} in the representation space. The corresponding first-order directional derivative can be approximated as

$$\mathcal{L}(u + \varepsilon e, y) \approx \mathcal{L}(u, y) + \varepsilon \langle \nabla_u \mathcal{L}(u, y), e \rangle, \quad (\varepsilon \rightarrow 0^+), \quad (1)$$

where e denotes a unit direction vector. This formulation naturally motivates the following definitions.

Harmful direction. A direction is considered harmful if an infinitesimal positive perturbation along it increases the loss. For a canonical basis vector e_j ,

$$\frac{\partial \mathcal{L}}{\partial u_j} > 0 \Leftrightarrow \mathcal{L}(u + \varepsilon e_j, y) > \mathcal{L}(u, y) \quad (\varepsilon \rightarrow 0^+), \quad (2)$$

where $u_j = \langle u, e_j \rangle$. Thus, coordinates with $\frac{\partial \mathcal{L}}{\partial u_j} > 0$ correspond to harmful components at the current point. In vector form, we define the positive part of the gradient as

$$g^+ \triangleq [\nabla_u \mathcal{L}]_+, \quad ([a]_+)_j = \max(a_j, 0), \quad (3)$$

so that g^+ aggregates all harmful coordinates into a unified composite direction.

Beneficial direction. Analogously, a beneficial direction corresponds to a perturbation that locally decreases the loss. We define the negative part of the gradient as

$$g^- \triangleq [\nabla_u \mathcal{L}]_-, \quad ([a]_-)_j = \min(a_j, 0), \quad (4)$$

so that g^- captures the composite direction that induces a local loss reduction under a positive perturbation.

Summary. In summary, g^+ characterizes the local half-space of coordinates whose activations should be suppressed, whereas g^- identifies the complementary half-space that can be encouraged to facilitate optimization.

4. Methodology

The overall framework of the proposed DGS-Net is depicted in Figure 2. It consists of two core components: **Orthogonal Suppression** and **Prior Alignment**. These modules respectively aim to suppress task-irrelevant representations and preserve transferable priors established during large-scale pre-training. Specifically, in *Orthogonal Suppression*, the image gradients of the training network are orthogonally projected onto the subspace complementary to the harmful directions inferred from text gradients, thereby mitigating cross-modal interference. In *Prior Alignment*, the coordinate-wise negative components of the frozen CLIP image gradients are introduced as lightweight alignment signals to reinforce beneficial pre-trained priors. The subsequent section provides a detailed methodological description, elaborating on the design principles and key mechanisms that underlie DGS-Net.

4.1. Notation and Setup

Given image-label pair (x, y) with $y \in \{0, 1\}$, where $y = 1$ denotes a *fake* image and $y = 0$ denotes a *real* image, CLIP provides an image encoder E_{img} and a text encoder E_{text} . The corresponding feature extraction processes are defined as:

$$f = E_{\text{img}}(x; \theta) \in \mathbb{R}^d, \quad t = E_{\text{text}}(z; \phi) \in \mathbb{R}^d, \quad (5)$$

where θ denotes the trainable parameters of the image encoder, and ϕ is frozen since the text encoder is only used to extract semantic representations. Here, z represents the text description associated with image x . In this work, we incorporate LoRA (Low-Rank Adaptation) layers as the trainable parameters θ for fine-tuning CLIP’s image encoder, while using BLIP [40] to automatically generate the corresponding

text description z . Additionally, we maintain a frozen image encoder E_{img}^T —a copy of the CLIP image encoder prior to fine-tuning—to extract reference features:

$$f^T = E_{\text{img}}^T(x) \in \mathbb{R}^d. \quad (6)$$

We employ the BCEWithLogits loss for all branches, formulated as:

$$\begin{aligned} \mathcal{L}_{\text{img}} &= \ell(h_{\text{img}}(f), y), & \mathcal{L}_{\text{text}} &= \ell(h_{\text{text}}(t), y), \\ \mathcal{L}_{\text{img}}^T &= \ell(h_{\text{img}}^T(f^T), y), \end{aligned} \quad (7)$$

where h_{img} , h_{text} , and h_{img}^T denote linear classification heads. The corresponding gradients with respect to the feature representations are given by

$$\begin{aligned} g_{\text{task}} &= \nabla_f \mathcal{L}_{\text{img}} \in \mathbb{R}^d, & g_{\text{text}} &= \nabla_t \mathcal{L}_{\text{text}} \in \mathbb{R}^d, \\ g_{\text{img}} &= \nabla_{f^T} \mathcal{L}_{\text{img}}^T \in \mathbb{R}^d. \end{aligned} \quad (8)$$

4.2. Orthogonal Suppression

To effectively suppress task-irrelevant components, it is crucial to first characterize these irrelevant features. Since CLIP is trained for text–image alignment, the visual representations produced by its image encoder inherently contain rich semantic information. Prior studies have explored different ways to handle such semantics: some works [70, 89] exploit them to enhance model generalization, whereas others [87, 96] seek to eliminate them in order to emphasize low-level artifact cues. To further investigate the influence of semantic features on AI-generated image detection, we convert each image into a textual description and perform binary classification using only the text features extracted by the text encoder. As illustrated in Figure 3, this approach achieves an accuracy of approximately 60%, suggesting that semantic information indeed carries label-related signals. However, the majority of these semantics act as distractors, reflecting dataset-specific shortcuts that hinder generalization. Therefore, we infer that the semantic priors embedded in CLIP’s visual encoder contain substantial harmful knowledge from pre-training, which interferes with reliable detection of AI-generated images.

Therefore, we extract the harmful gradients from the text branch to suppress pre-trained components that are irrelevant to the detection task. As discussed in Sec. 3, if the text-branch gradient g_{text} is positive in a given dimension, a small positive perturbation along that coordinate will increase the loss. Consequently, gradient descent will update the corresponding semantic coordinate in the negative direction to reduce the loss. However, this behavior—*i.e.*, relying on semantic coordinates to minimize the loss—often reflects dataset-specific correlations rather than genuine forensic cues, thereby degrading cross-generator generalization. To address this issue, we regard the positive half-space of the

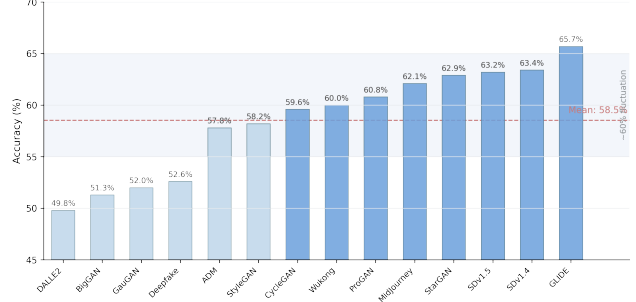


Figure 3. **Classification using only text descriptions achieves an accuracy of approximately 60%.** We used BLIP to convert images into textual descriptions and trained the detector directly on these text inputs. The resulting detection accuracy fluctuated around 60%, indicating that semantic information indeed carries label-related signals. However, most of them act as distractors, reflecting dataset-specific shortcuts that hinder cross-generator generalization.

text gradient as a **harmful direction** that should be suppressed, formulated as:

$$g_{\text{harm}} \triangleq g_{\text{text}}^+ = [\nabla_t \mathcal{L}_{\text{text}}]_+ \in \mathbb{R}^d. \quad (9)$$

We then seek an update direction \tilde{g} for the image representation that excludes the component aligned with g_{harm} . Following the principle of minimum deviation, this can be expressed as an optimization problem with an orthogonality constraint:

$$\begin{aligned} \Delta f^* &= \arg \min_{\Delta f} \frac{1}{2} \|\Delta f - g_{\text{task}}\|_2^2 \quad \text{s.t.} \quad \langle \Delta f, \hat{g}_{\text{harm}} \rangle = 0, \\ \hat{g}_{\text{harm}} &= \frac{g_{\text{harm}}}{\|g_{\text{harm}}\|_2}. \end{aligned} \quad (10)$$

The closed-form Lagrangian solution is given by

$$\tilde{g} \triangleq \Delta f^* = (I - \hat{g}_{\text{harm}} \hat{g}_{\text{harm}}^T) g_{\text{task}}, \quad (11)$$

where the projection operator $(I - \hat{g}_{\text{harm}} \hat{g}_{\text{harm}}^T)$ removes the harmful component, ensuring that the update direction is orthogonal to the undesired semantic subspace.

After applying orthogonal suppression, the gradient update direction shifts from g_{task} to \tilde{g} , effectively removing harmful semantic components from the image-task gradient. More importantly, different from existing methods [87, 96] that directly discard all semantic information, our approach only modifies the gradient update direction to be orthogonal to the harmful semantic component. In this way, we retain beneficial semantic cues while simultaneously improving the model’s generalization ability.

4.3. Prior Alignment

Similar to the approach described in Sec. 4.2, we define the negative direction of the image gradient as the *beneficial*

Detection Method	Real Image	Generative Adversarial Networks							Other		Diffusion Models							mAcc.	
		Pro-GAN	Cycle-GAN	Big-GAN	Style-GAN	Style-GAN2	Gau-GAN	Star-GAN	WFIR	Deep-fake	SDv1.4	SDv1.5	ADM	GLIDE	Mid-journey	Wukong	VQDM		DALLE2
CNN-Spot [77]	99.0	95.3	18.7	1.8	36.5	22.0	2.5	23.1	1.1	29.3	55.9	55.6	1.8	4.8	5.2	27.6	0.7	4.5	29.0
UnivFD [55]	92.3	98.9	90.5	79.2	55.7	48.7	91.1	96.9	92.8	26.9	96.3	96.0	12.7	75.6	61.2	84.7	45.6	62.3	72.7
FreqNet [68]	89.9	99.4	57.1	51.0	75.1	67.5	9.9	88.4	<u>95.4</u>	35.8	99.9	99.8	37.7	78.9	80.8	98.0	34.1	88.8	71.7
NPR [69]	99.3	98.9	29.3	16.5	67.1	58.7	1.7	6.5	7.9	0.1	100.0	99.9	26.5	69.2	71.0	97.7	15.4	89.8	53.1
Ladeda [2]	99.8	99.7	7.2	29.0	95.6	98.3	4.9	0.0	19.2	0.1	100.0	99.9	27.3	79.7	<u>88.8</u>	97.9	15.5	92.4	58.6
AIDE [88]	93.0	95.3	88.0	96.9	89.6	97.0	90.0	97.0	42.9	9.2	99.8	99.7	<u>92.4</u>	<u>98.7</u>	63.7	98.9	90.1	<u>98.9</u>	85.6
C2P-CLIP* [70]	<u>99.8</u>	100.0	99.8	99.8	72.2	78.0	87.7	100.0	34.9	67.6	100.0	99.9	50.5	73.3	<u>28.4</u>	99.7	93.3	98.1	82.4
DFFreq [86]	98.0	98.0	70.9	93.6	<u>99.0</u>	<u>98.9</u>	<u>93.8</u>	97.4	3.5	76.0	99.9	99.8	65.9	87.8	94.8	99.1	76.0	95.9	85.2
SAFE [42]	99.2	99.7	85.6	83.5	88.1	96.7	89.0	99.9	8.4	17.3	99.8	99.6	36.8	90.5	86.3	98.5	84.0	92.0	80.8
Effort [89]	99.8	100.0	<u>100.0</u>	100.0	79.6	82.1	<u>100.0</u>	<u>100.0</u>	99.9	<u>76.6</u>	100.0	99.9	53.1	81.2	44.2	99.9	96.3	75.8	88.1
NS-Net [87]	97.7	<u>100.0</u>	99.9	<u>100.0</u>	95.7	98.6	98.5	<u>100.0</u>	68.9	<u>60.6</u>	<u>100.0</u>	<u>99.9</u>	85.3	97.2	77.4	<u>100.0</u>	<u>98.9</u>	98.8	<u>93.2</u>
Ours	95.3	100.0	100.0	100.0	99.5	99.8	100.0	100.0	84.6	96.7	100.0	99.9	95.2	99.0	88.0	100.0	99.7	99.6	97.6

Table 1. **Cross-model Accuracy (Acc.) Performance on the GenImage [100] Dataset.** The first column represents the accuracy of detecting real images (R.Acc.), and the others are the accuracy of detecting fake images (F.Acc.).

Detection Method	Generative Adversarial Networks							Other		Diffusion Models							mA.P.	
	Pro-GAN	Cycle-GAN	Big-GAN	Style-GAN	Style-GAN2	Gau-GAN	Star-GAN	WFIR	Deep-fake	SDv1.4	SDv1.5	ADM	GLIDE	Mid-journey	Wukong	VQDM		DALLE2
CNN-Spot [77]	99.9	91.0	59.2	94.8	94.2	86.1	82.5	65.5	74.2	97.6	97.6	66.6	83.1	80.4	88.9	57.0	87.8	84.3
UnivFD [55]	99.9	96.2	94.7	90.9	91.1	97.6	99.7	83.0	83.5	99.3	99.1	65.2	95.3	91.7	97.4	87.2	89.8	91.9
FreqNet [68]	100.0	97.5	87.9	95.9	94.2	54.0	100.0	57.0	88.5	99.9	99.9	73.9	94.1	94.4	99.1	74.9	92.3	88.4
NPR [69]	100.0	98.6	79.4	98.6	99.6	71.3	97.6	65.5	92.5	100.0	99.9	74.1	97.4	97.8	99.9	81.5	99.3	91.4
Ladeda [2]	100.0	99.0	89.5	100.0	100.0	96.4	90.3	93.6	92.6	95.5	95.8	84.8	96.6	93.5	93.0	84.5	93.9	94.0
AIDE [88]	99.6	98.2	91.6	99.4	99.9	74.1	99.7	90.8	66.5	99.9	99.9	99.4	99.9	90.3	99.9	98.9	99.9	94.5
C2P-CLIP* [70]	100.0	100.0	99.9	99.3	99.7	98.8	100.0	99.6	<u>98.3</u>	100.0	100.0	96.3	98.9	90.4	100.0	99.9	100.0	98.8
DFFreq [86]	100.0	98.7	98.4	<u>100.0</u>	100.0	98.1	99.8	89.0	87.5	100.0	99.9	98.7	99.5	<u>99.7</u>	100.0	99.3	99.9	98.1
SAFE [42]	100.0	99.5	97.8	99.9	<u>100.0</u>	96.6	100.0	73.8	91.0	100.0	100.0	98.1	<u>99.9</u>	99.9	100.0	99.9	100.0	97.4
Effort [89]	100.0	100.0	100.0	99.3	99.2	100.0	100.0	91.1	97.9	100.0	100.0	97.5	99.8	98.9	100.0	100.0	99.9	99.0
NS-Net [87]	<u>100.0</u>	<u>100.0</u>	99.7	99.8	99.9	97.0	<u>100.0</u>	99.5	95.2	<u>100.0</u>	<u>100.0</u>	100.0	99.8	97.0	<u>100.0</u>	<u>100.0</u>	<u>100.0</u>	99.2
Ours	100.0	100.0	99.9	100.0	100.0	98.8	100.0	99.8	98.3	100.0	100.0	99.8	100.0	99.6	100.0	100.0	100.0	99.8

Table 2. **Cross-model Average Precision (A.P.) Performance on the GenImage [100] Dataset.**

direction, expressed as:

$$g_{\text{help}} \triangleq g_{\text{img}}^- = [\nabla_{f^T} \mathcal{L}_{\text{img}}^T]_- \in \mathbb{R}^d, \quad (12)$$

which provides effective descent guidance toward downstream objectives while preserving the priors learned during pre-training.

To further maintain the transferable priors and geometric structures established by CLIP’s pre-training, we introduce a linear alignment regularization term at the feature level:

$$\mathcal{L}_{\text{align}} = \langle f, g_{\text{help}} \rangle, \quad (13)$$

whose gradient with respect to f is:

$$\nabla_f \mathcal{L}_{\text{align}} = g_{\text{help}}. \quad (14)$$

In essence, this mechanism injects beneficial descent directions derived from the pre-trained model into the fine-tuning process, thereby promoting lightweight alignment with transferable priors and enhancing the model’s overall detection capability.

4.4. Overall Process and Loss Function

The overall training objective of DGS-Net is formulated as:

$$\mathcal{L} = \mathcal{L}_{\text{img}} + \mathcal{L}_{\text{text}} + \lambda \mathcal{L}_{\text{align}}, \quad (15)$$

where λ is hyperparameter that balances the alignment term.

During backpropagation, the gradient propagated to the image feature f is replaced by

$$g_{\text{final}} = \underbrace{(I - \hat{g}_{\text{harm}} \hat{g}_{\text{harm}}^T)}_{\text{Orthogonal Suppression}(\hat{g})} \nabla_f \mathcal{L}_{\text{img}} + \underbrace{\lambda g_{\text{help}}}_{\text{Prior Alignment}}, \quad (16)$$

which jointly enforces semantic suppression and prior preservation. By the chain rule, the parameter update can be expressed as:

$$\theta \leftarrow \theta - \mu \left(\frac{\partial E_{\text{img}}(x; \theta)}{\partial \theta} \right)^T g_{\text{final}}, \quad (17)$$

where μ denotes the learning rate. Through the integration of *Orthogonal Suppression* and *Prior Alignment*, the feature extractor E_{img} not only mitigates harmful semantic interference but also retains transferable pre-training priors, thereby enhancing generalization in AI-generated image detection.

During training, we update only the LoRA parameters of the CLIP image encoder (θ) and the two classification heads, h_{img} and h_{text} , while keeping all other parameters frozen. At inference time, only the image encoder E_{img} and the linear classification head h_{img} are used for image detection, ensuring computational efficiency.

Generator	CNN-Spot	UnivFD	FreqNet	NPR	Ladeda	AIDE	C2P-CLIP*	DFFreq	SAFE	Effort	NS-Net	Ours
Real Image	<u>98.2</u>	73.3	64.6	93.8	91.7	88.1	93.8	99.3	92.4	96.9	88.3	83.0
ProGAN	95.3	98.9	99.4	98.9	99.7	95.3	100.0	78.4	99.7	100.0	<u>100.0</u>	100.0
R3GAN	2.3	94.1	59.9	8.4	19.5	<u>99.0</u>	69.0	78.4	93.0	94.4	98.5	99.9
StyleGAN3	9.1	82.6	98.2	63.6	93.2	91.1	99.2	95.5	94.6	95.0	<u>99.6</u>	99.7
StyleGAN-XL	0.7	96.7	95.5	28.2	80.5	91.7	99.9	15.6	89.4	82.3	99.3	<u>99.6</u>
StyleSwim	6.9	98.1	97.1	77.7	97.3	82.0	99.8	99.8	<u>99.9</u>	97.6	99.8	99.9
WFIR	1.1	<u>92.8</u>	95.4	7.9	19.2	42.9	34.9	3.5	8.4	91.1	69.3	84.5
BlendFace	6.2	5.5	0.3	0.0	0.0	<u>23.2</u>	3.8	1.5	2.6	11.2	16.2	69.6
E4S	4.1	46.9	1.1	0.0	0.0	6.6	0.6	1.2	1.3	18.2	4.4	<u>44.8</u>
FaceSwap	1.4	<u>27.3</u>	6.2	0.0	0.0	14.3	4.6	7.4	3.0	14.1	11.1	66.6
InSwap	9.7	8.2	0.9	0.0	0.0	11.4	5.5	2.8	1.9	<u>17.3</u>	16.9	70.7
SimSwap	6.2	8.6	0.6	0.0	0.0	21.5	8.4	1.8	2.5	<u>35.2</u>	21.7	81.4
DALLE-3	9.8	75.2	<u>68.2</u>	21.2	9.7	24.5	0.7	3.4	0.5	12.9	0.1	2.8
FLUX1-dev	16.3	86.6	92.4	97.2	<u>99.3</u>	90.0	41.2	96.1	99.5	26.8	96.2	98.7
Midjourney-V6	5.8	80.6	83.6	53.8	83.4	79.8	67.3	<u>95.8</u>	94.1	70.4	94.8	97.7
GLIDE	4.6	75.2	79.7	70.3	81.8	<u>98.4</u>	70.7	86.9	89.2	81.0	96.6	98.6
Imagen3	4.2	84.2	81.5	78.2	92.6	93.9	71.7	51.9	94.8	84.8	99.5	<u>99.4</u>
SD3	13.3	90.6	88.1	89.7	99.0	99.3	83.7	92.1	94.4	86.9	99.9	<u>99.8</u>
SDXL	7.2	88.0	98.9	79.0	98.3	97.6	84.4	98.0	99.9	86.4	<u>99.9</u>	100.0
BLIP	56.5	92.1	100.0	99.9	100.0	100.0	100.0	100.0	100.0	100.0	<u>100.0</u>	100.0
Infinite-ID	1.1	93.8	92.7	34.6	32.2	97.5	36.5	93.9	<u>99.2</u>	43.3	92.2	99.8
PhotoMaker	1.7	65.2	88.6	3.6	66.7	97.5	23.5	<u>99.6</u>	99.7	23.2	41.9	96.6
Instant-ID	8.1	96.9	93.9	34.1	82.4	97.0	38.4	<u>100.0</u>	100.0	46.2	78.9	98.7
IP-Adapter	6.0	92.0	92.0	71.8	90.6	93.5	82.1	97.8	97.2	88.2	<u>99.8</u>	99.9
SocialRF	7.5	55.5	<u>39.3</u>	21.9	19.4	18.4	14.3	18.4	17.1	16.9	18.4	19.2
CommunityAI	5.4	51.2	<u>12.2</u>	8.2	9.0	9.3	5.2	9.2	9.1	5.2	8.9	9.2
Average	15.0	<u>71.5</u>	66.6	43.9	56.4	67.8	51.5	58.8	64.7	58.7	67.4	81.6

Table 3. **Cross-model Accuracy (Acc.) Performance on the AIGIBench [47] Dataset.** The first row represents the accuracy of detecting real images (R.Acc.), and the others are the accuracy of detecting fake images (F.Acc.).

5. Experiments

5.1. Settings

Training datasets. We adopt the **Setting-II** of AIGIBench [47], which includes 144k images generated by ProGAN [33] and SDv1.4 [63], along with real images.

Testing datasets. To comprehensively evaluate the effectiveness of our method, we use three benchmarks for detection analysis, including UniversalFakeDetect (shown in Sec. 8 of the Appendix), GenImage, and AIGIBench. The UniversalFakeDetect [55] contains 8 subsets from various generative models, including Guided [17], GLIDE [54], LDM [63] and DALLE [61]. The GenImage [100] datasets comprise 17 generators, including ProGAN [33], CycleGAN [99], BigGAN [1], StyleGAN [32], StyleGAN2 [34], GauGAN [57], StarGAN [13], WFIR [81], Deepfake [64], SDv1.4 [63], SDv1.5 [63], ADM [17], GLIDE [54], Midjourney [72], Wukong [85], VQDM [21] and DALLE2 [62]. The AIGIBench [47] includes more comprehensive and advanced generative models, including ProGAN [33], R3GAN [28], StyleGAN3 [35], StyleGAN-XL [65], StyleSwim [95], WFIR [81], BlendFace [66], E4S [49], FaceSwap [52], InSwap [75], SimSwap [9], DALLE-3 [73], FLUX1-dev [39], Midjourney-V6 [72], GLIDE [54], Imagen3 [16], SD3 [18], SDXL [59],

BLIP [40], Infinite-ID [84], PhotoMaker [46], Instant-ID [76], IP-Adapter [92], CommunityAI and SocialRF.

Implementation Details. Our method is implemented using the PyTorch framework on an NVIDIA RTX 4090 GPU. The model is trained with the Adam optimizer [37], a learning rate of 1×10^{-4} , and a batch size of 32 for only 1 epoch. The ViT-L/14 model of CLIP is adopted as the pre-trained model [55]. In addition, we add Low-Rank Adaptation to fine-tune the CLIP’s image encoder, following [94]. We configure the hyperparameters of the LoRA layers as follows: `lora_r = 6`, `lora_alpha = 6`, and `lora_dropout = 0.8`. The hyperparameter λ is set to 0.2. We use Patch Selection [87] as data preprocessing to resize the image to 224×224 . Importantly, to ensure a fair comparison, we retrain all baseline methods ¹ on the same training set described above. More details are shown in Sec. 7 of the Appendix.

5.2. Comparison with the State-of-the-Art

Evaluation on GenImage. The results of accuracy (Acc.) and average precision (A.P.) are shown in Table 1 and 2 respectively. Overall, our method achieves 97.6% mAcc. and 99.8% mA.P. across 17 test subsets. Although infer-

¹When training C2P-CLIP [70], we replace the original text generation module (ClipCap) with BLIP, keeping all other components unchanged.

Orthogonal Suppression	Prior Alignment	GenImage [100]	AIGIBench [47]
\times	\times	79.9	52.4
\times	\checkmark	83.3 _{+3.4}	58.0 _{+5.6}
\checkmark	\times	88.0 _{+8.1}	61.7 _{+9.3}
\checkmark	\checkmark	97.6_{+17.7}	81.6_{+29.2}

Table 4. **Ablation Study of our method.** The accuracy averaged on the GenImage [100] and AIGIBench [47] datasets.

ence remains identical to C2P-CLIP, our method improves 15.2% mAcc. and 1.0% mA.P., indicating a substantial improvement in CLIP-based detection. Furthermore, compared with the state-of-the-art, NS-Net, our method achieves an additional 4.4% improvement in accuracy. Notably, on the challenging Deepfake dataset, it reaches 96.7% in accuracy, whereas existing methods have historically shown very low performance on this dataset.

Evaluation on AIGIBench. We show the results of accuracy (Acc.) on the AIGIBench dataset in Table 3. The additional metric about A.P. is shown in the Sec. 9 of the Appendix. Our method achieves 81.6% accuracy, representing a 10.1% improvement over the state-of-the-art, UnivFD. Notably, for Deepfake datasets such as BlendFace, where existing detection methods almost completely fail, our method delivers a substantial gain with an average accuracy improvement of about 50%. Nevertheless, performance remains poor on certain datasets (DALLE-3, SocialRF, CommunityAI), similar to other methods. This may be attributed to unknown post-processing operations, which remain an open challenge.

5.3. Ablation Studies

To further assess the effectiveness of our network, we perform ablation studies on its core components, including Orthogonal Suppression and Prior Alignment. The corresponding results are shown in Table 4. Compared with the baseline, our method achieves 17.7% and 29.2% improvements in accuracy on the GenImage [100] and AIGIBench [47] datasets, respectively. This demonstrates that our method substantially enhances CLIP’s ability to extract more generalizable artifact representations for universal AI-generated image detection. Moreover, the inclusion of any single component yields measurable performance gains, further demonstrating the effectiveness of our approach in addressing the challenges of catastrophic forgetting. More ablation studies are shown in Sec. 10 of the Appendix.

5.4. Robustness Evaluation

In real-world scenarios, images are inevitably affected by unknown disturbances during transmission and interaction, which pose additional challenges for AI-generated image detection. To investigate robustness under such conditions, we further evaluate the performance of different detection

Method	JPEG Compression			Gaussian Blur		
	QF=95	QF=85	QF=75	$\sigma = 0.5$	$\sigma = 1.0$	$\sigma = 1.5$
CNN-Spot [77]	59.0	59.9	60.5	62.4	63.2	63.3
UnivFD[55]	76.4	74.2	73.8	80.2	76.8	76.3
NPR [69]	72.8	70.7	69.2	80.6	79.6	81.0
AIDE [88]	74.6	74.1	70.3	88.6	75.8	81.1
SAFE [42]	57.7	59.6	60.4	88.5	80.6	83.0
NS-Net [87]	85.6	82.3	79.6	88.8	86.1	85.9
Ours	88.9	85.0	82.4	92.7	89.7	89.9

Table 5. **Robustness on JPEG Compression and Gaussian Blur of Our Method.** The accuracy (%) averaged on GenImage [100].

Method	JPEG Compression			Gaussian Blur		
	QF=95	QF=85	QF=75	$\sigma = 0.5$	$\sigma = 1.0$	$\sigma = 1.5$
CNN-Spot [77]	53.8	54.3	54.5	56.5	56.5	56.6
UnivFD[55]	65.6	66.3	65.1	72.2	68.6	68.6
NPR [69]	59.0	58.9	58.6	62.9	62.0	62.9
AIDE [88]	61.0	59.6	55.9	75.5	63.4	65.2
SAFE [42]	51.3	47.9	47.8	75.5	67.6	69.3
NS-Net [87]	68.9	67.1	64.9	72.8	70.3	70.2
Ours	69.4	67.8	65.7	75.4	72.9	73.1

Table 6. **Robustness on JPEG Compression and Gaussian Blur of Our Method.** The accuracy (%) averaged on AIGIBench [47].

methods against a variety of disturbances, such as JPEG compression and Gaussian blur. As illustrated in Table 5 and 6, experiments on two different datasets show that all methods suffer performance degradation under perturbations, which weakens the detectors’ ability to reliably distinguish real from fake images. Despite these challenging conditions, our method consistently outperforms competing approaches, maintaining relatively high accuracy. Notably, our method exhibits almost no degradation in detection performance under varying levels of Gaussian blur interference, further demonstrating its strong robustness.

6. Conclusion

In this paper, we review and analyze existing strategies for fine-tuning CLIP in AI-generated image detection, and identify that catastrophic forgetting in current fine-tuning paradigms undermines the transferable priors of the pre-trained model. To address these challenges, we propose a novel Distillation-Guided Gradient Surgery Network (DGS-Net). Specifically, we orthogonally project the image gradients of the training network onto the complement of the harmful directions estimated from text gradients, thereby suppressing components irrelevant to the detection. In addition, we inject the coordinate-wise negative component of a frozen CLIP’s image gradients as a lightweight alignment, thus preserving the transferable priors and geometric structure established during large-scale pre-training. Together, they strike a balance between suppressing irrelevance and preserving transferable priors, substantially enhancing the generalization performance of AI-generated image detection.

References

- [1] Andrew Brock. Large scale gan training for high fidelity natural image synthesis. *arXiv preprint arXiv:1809.11096*, 2018. 7
- [2] Bar Cavia, Eliahu Horwitz, Tal Reiss, and Yedid Hoshen. Real-time deepfake detection in the real-world. *arXiv preprint arXiv:2406.09398*, 2024. 3, 6, 1, 2
- [3] George Cazenavette, Avneesh Sud, Thomas Leung, and Ben Usman. Fakeinversion: Learning to detect images from unseen text-to-image models by inverting stable diffusion. In *Proceedings of the IEEE/CVF Conference on Computer Vision and Pattern Recognition*, pages 10759–10769, 2024. 3
- [4] Lucy Chai, David Bau, Ser-Nam Lim, and Phillip Isola. What makes fake images detectable? understanding properties that generalize. In *Computer Vision—ECCV 2020: 16th European Conference, Glasgow, UK, August 23–28, 2020, Proceedings, Part XXVI 16*, pages 103–120. Springer, 2020. 3
- [5] Baoying Chen, Jishen Zeng, Jianquan Yang, and Rui Yang. Drct: Diffusion reconstruction contrastive training towards universal detection of diffusion generated images. In *Forty-first International Conference on Machine Learning*, 2024. 3
- [6] Guobin Chen, Wongun Choi, Xiang Yu, Tony Han, and Manmohan Chandraker. Learning efficient object detection models with knowledge distillation. *Advances in neural information processing systems*, 30, 2017. 3
- [7] Mengxi Chen, Linyu Xing, Yu Wang, and Ya Zhang. Enhanced multimodal representation learning with cross-modal kd. In *Proceedings of the IEEE/CVF Conference on Computer Vision and Pattern Recognition*, pages 11766–11775, 2023. 3
- [8] Pengguang Chen, Shu Liu, Hengshuang Zhao, and Jiaya Jia. Distilling knowledge via knowledge review. In *Proceedings of the IEEE/CVF conference on computer vision and pattern recognition*, pages 5008–5017, 2021. 3
- [9] Renwang Chen, Xuanhong Chen, Bingbing Ni, and Yanhao Ge. Simswap: An efficient framework for high fidelity face swapping. In *Proceedings of the 28th ACM international conference on multimedia*, pages 2003–2011, 2020. 1, 7
- [10] Ruoxin Chen, Junwei Xi, Zhiyuan Yan, Ke-Yue Zhang, Shuang Wu, Jingyi Xie, Xu Chen, Lei Xu, Isabel Guan, Taiping Yao, et al. Dual data alignment makes ai-generated image detector easier generalizable. *arXiv preprint arXiv:2505.14359*, 2025. 3
- [11] Yifan Chen, Xiaozhen Qiao, Zhe Sun, and Xuelong Li. Comkd-clip: Comprehensive knowledge distillation for contrastive language-image pre-training model. *arXiv preprint arXiv:2408.04145*, 2024. 3
- [12] Zehao Chen and Hua Yang. Manipulated face detector: Joint spatial and frequency domain attention network. *arXiv preprint arXiv:2005.02958*, 1(2):4, 2020. 3
- [13] Yunjey Choi, Minje Choi, Munyoung Kim, Jung-Woo Ha, Sunghun Kim, and Jaegul Choo. Stargan: Unified generative adversarial networks for multi-domain image-to-image translation. In *Proceedings of the IEEE conference on computer vision and pattern recognition*, pages 8789–8797, 2018. 7
- [14] Beilin Chu, Xuan Xu, Xin Wang, Yufei Zhang, WeiKe You, and Linna Zhou. Fire: Robust detection of diffusion-generated images via frequency-guided reconstruction error. In *Proceedings of the Computer Vision and Pattern Recognition Conference*, pages 12830–12839, 2025. 3
- [15] Xing Dai, Zeren Jiang, Zhao Wu, Yiping Bao, Zhicheng Wang, Si Liu, and Erjin Zhou. General instance distillation for object detection. In *Proceedings of the IEEE/CVF conference on computer vision and pattern recognition*, pages 7842–7851, 2021. 3
- [16] Google DeepMind. Imagen3. <https://deepmind.google/technologies/imagen-3>. 2024. 7
- [17] Prafulla Dhariwal and Alexander Nichol. Diffusion models beat gans on image synthesis. *Advances in neural information processing systems*, 34:8780–8794, 2021. 2, 7
- [18] Patrick Esser, Sumith Kulal, Andreas Blattmann, Rahim Entezari, Jonas Müller, Harry Saini, Yam Levi, Dominik Lorenz, Axel Sauer, Frederic Boesel, et al. Scaling rectified flow transformers for high-resolution image synthesis. In *Forty-first international conference on machine learning*, 2024. 7
- [19] Zhiyuan Fang, Jianfeng Wang, Xiaowei Hu, Lijuan Wang, Yezhou Yang, and Zicheng Liu. Compressing visual-linguistic model via knowledge distillation. In *Proceedings of the IEEE/CVF International Conference on Computer Vision*, pages 1428–1438, 2021. 3
- [20] Xinghe Fu, Zhiyuan Yan, Taiping Yao, Shen Chen, and Xi Li. Exploring unbiased deepfake detection via token-level shuffling and mixing. In *Proceedings of the AAAI Conference on Artificial Intelligence*, pages 3040–3048, 2025. 1
- [21] Shuyang Gu, Dong Chen, Jianmin Bao, Fang Wen, Bo Zhang, Dongdong Chen, Lu Yuan, and Baining Guo. Vector quantized diffusion model for text-to-image synthesis. In *Proceedings of the IEEE/CVF conference on computer vision and pattern recognition*, pages 10696–10706, 2022. 7
- [22] Fabrizio Guillaro, Giada Zingarini, Ben Usman, Avneesh Sud, Davide Cozzolino, and Luisa Verdoliva. A bias-free training paradigm for more general ai-generated image detection. In *Proceedings of the Computer Vision and Pattern Recognition Conference*, pages 18685–18694, 2025. 3
- [23] Byeongho Heo, Jeesoo Kim, Sangdoo Yun, Hyojin Park, Nojun Kwak, and Jin Young Choi. A comprehensive overhaul of feature distillation. In *Proceedings of the IEEE/CVF international conference on computer vision*, pages 1921–1930, 2019. 3
- [24] Geoffrey Hinton, Oriol Vinyals, and Jeff Dean. Distilling the knowledge in a neural network. *arXiv preprint arXiv:1503.02531*, 2015. 2, 3
- [25] Jonathan Ho, Ajay Jain, and Pieter Abbeel. Denoising diffusion probabilistic models. *Advances in neural information processing systems*, 33:6840–6851, 2020. 1, 2
- [26] Edward J Hu, Yelong Shen, Phillip Wallis, Zeyuan Allen-Zhu, Yuanzhi Li, Shean Wang, Lu Wang, Weizhu Chen, et al. Lora: Low-rank adaptation of large language models. *ICLR*, 1(2):3, 2022. 1

- [27] Libo Huang, Yan Zeng, Chuanguang Yang, Zhulin An, Boyu Diao, and Yongjun Xu. etag: Class-incremental learning via embedding distillation and task-oriented generation. In *Proceedings of the AAAI Conference on Artificial Intelligence*, pages 12591–12599, 2024. 3
- [28] Nick Huang, Aaron Gokaslan, Volodymyr Kuleshov, and James Tompkin. The gan is dead; long live the gan! a modern gan baseline. *Advances in Neural Information Processing Systems*, 37:44177–44215, 2024. 1, 2, 7
- [29] Yonghyun Jeong, Doyeon Kim, Seungjai Min, Seongho Joe, Youngjune Gwon, and Jongwon Choi. Bihpf: Bilateral high-pass filters for robust deepfake detection. In *Proceedings of the IEEE/CVF Winter Conference on Applications of Computer Vision*, pages 48–57, 2022. 3
- [30] Zihao Jia, Shengkun Sun, Guangcan Liu, and Bo Liu. Mssd: multi-scale self-distillation for object detection. *Visual Intelligence*, 2(1):8, 2024. 3
- [31] Xiaoqi Jiao, Yichun Yin, Lifeng Shang, Xin Jiang, Xiao Chen, Linlin Li, Fang Wang, and Qun Liu. Tinybert: Distilling bert for natural language understanding. *arXiv preprint arXiv:1909.10351*, 2019. 3
- [32] Tero Karras. A style-based generator architecture for generative adversarial networks. *arXiv preprint arXiv:1812.04948*, 2019. 7
- [33] Tero Karras, Timo Aila, Samuli Laine, and Jaakko Lehtinen. Progressive growing of GANs for improved quality, stability, and variation. In *International Conference on Learning Representations*, 2018. 1, 2, 7
- [34] Tero Karras, Samuli Laine, Miika Aittala, Janne Hellsten, Jaakko Lehtinen, and Timo Aila. Analyzing and improving the image quality of stylegan. In *Proceedings of the IEEE/CVF conference on computer vision and pattern recognition*, pages 8110–8119, 2020. 7
- [35] Tero Karras, Miika Aittala, Samuli Laine, Erik Härkönen, Janne Hellsten, Jaakko Lehtinen, and Timo Aila. Alias-free generative adversarial networks. *Advances in neural information processing systems*, 34:852–863, 2021. 2, 7
- [36] Jangho Kim, SeongUk Park, and Nojun Kwak. Paraphrasing complex network: Network compression via factor transfer. *Advances in neural information processing systems*, 31, 2018. 3
- [37] Diederik P Kingma. Adam: A method for stochastic optimization. *arXiv preprint arXiv:1412.6980*, 2014. 3, 7
- [38] Christos Koutlis and Symeon Papadopoulos. Leveraging representations from intermediate encoder-blocks for synthetic image detection. In *European Conference on Computer Vision*, pages 394–411. Springer, 2024. 1, 3
- [39] Black Forest Labs. Flux.1-dev. <https://huggingface.co/black-forest-labs/FLUX.1-dev>. 2024. 7
- [40] Junnan Li, Dongxu Li, Caiming Xiong, and Steven Hoi. Blip: Bootstrapping language-image pre-training for unified vision-language understanding and generation. In *International conference on machine learning*, pages 12888–12900. PMLR, 2022. 4, 7
- [41] Manyi Li, Renshuai Tao, Yufan Liu, Chuangchuang Tan, Haotong Qin, Bing Li, Yunchao Wei, and Yao Zhao. Pay less attention to deceptive artifacts: Robust detection of compressed deepfakes on online social networks. *arXiv preprint arXiv:2506.20548*, 2025. 1
- [42] Ouxiang Li, Jiayin Cai, Yanbin Hao, Xiaolong Jiang, Yao Hu, and Fuli Feng. Improving synthetic image detection towards generalization: An image transformation perspective. In *Proceedings of the 31st ACM SIGKDD Conference on Knowledge Discovery and Data Mining V. 1*, pages 2405–2414, 2025. 3, 6, 8, 1, 2
- [43] Quanquan Li, Shengying Jin, and Junjie Yan. Mimicking very efficient network for object detection. In *Proceedings of the IEEE conference on computer vision and pattern recognition*, pages 6356–6364, 2017. 3
- [44] Zheng Li, Jingwen Ye, Mingli Song, Ying Huang, and Zhigeng Pan. Online knowledge distillation for efficient pose estimation. In *Proceedings of the IEEE/CVF international conference on computer vision*, pages 11740–11750, 2021. 3
- [45] Zheng Li, Xiang Li, Lingfeng Yang, Borui Zhao, Renjie Song, Lei Luo, Jun Li, and Jian Yang. Curriculum temperature for knowledge distillation. In *Proceedings of the AAAI Conference on Artificial Intelligence*, pages 1504–1512, 2023. 3
- [46] Zhen Li, Mingdeng Cao, Xintao Wang, Zhongang Qi, Ming-Ming Cheng, and Ying Shan. Photomaker: Customizing realistic human photos via stacked id embedding. In *Proceedings of the IEEE/CVF conference on computer vision and pattern recognition*, pages 8640–8650, 2024. 2, 7
- [47] Ziqiang Li, Jiazhen Yan, Ziwen He, Kai Zeng, Weiwei Jiang, Lizhi Xiong, and Zhangjie Fu. Is artificial intelligence generated image detection a solved problem? In *Advances in Neural Information Processing Systems*, 2025. 7, 8, 1, 2
- [48] Huan Liu, Zichang Tan, Chuangchuang Tan, Yunchao Wei, Jingdong Wang, and Yao Zhao. Forgery-aware adaptive transformer for generalizable synthetic image detection. In *Proceedings of the IEEE/CVF Conference on Computer Vision and Pattern Recognition*, pages 10770–10780, 2024. 1, 3
- [49] Zhian Liu, Maomao Li, Yong Zhang, Cairong Wang, Qi Zhang, Jue Wang, and Yongwei Nie. Fine-grained face swapping via regional gan inversion. In *Proceedings of the IEEE/CVF conference on computer vision and pattern recognition*, pages 8578–8587, 2023. 7
- [50] Zihan Liu, Hanyi Wang, Yaoyu Kang, and Shilin Wang. Mixture of low-rank experts for transferable ai-generated image detection. *arXiv preprint arXiv:2404.04883*, 2024. 3
- [51] Yuchen Luo, Yong Zhang, Junchi Yan, and Wei Liu. Generalizing face forgery detection with high-frequency features. In *Proceedings of the IEEE/CVF conference on computer vision and pattern recognition*, pages 16317–16326, 2021. 3
- [52] Marek. Faceswap. <https://github.com/MarekKowalski/FaceSwap>. 2020. 7
- [53] Roy Miles, Adrian Lopez Rodriguez, and Krystian Mikołajczyk. Information theoretic representation distillation. *arXiv preprint arXiv:2112.00459*, 2021. 3
- [54] Alex Nichol, Prafulla Dhariwal, Aditya Ramesh, Pranav Shyam, Pamela Mishkin, Bob McGrew, Ilya Sutskever, and

- Mark Chen. Glide: Towards photorealistic image generation and editing with text-guided diffusion models. *arXiv preprint arXiv:2112.10741*, 2021. 7
- [55] Utkarsh Ojha, Yuheng Li, and Yong Jae Lee. Towards universal fake image detectors that generalize across generative models. In *Proceedings of the IEEE/CVF Conference on Computer Vision and Pattern Recognition*, pages 24480–24489, 2023. 1, 3, 6, 7, 8, 2
- [56] Geondo Park, Gyeongman Kim, and Eunho Yang. Distilling linguistic context for language model compression. *arXiv preprint arXiv:2109.08359*, 2021. 3
- [57] Taesung Park, Ming-Yu Liu, Ting-Chun Wang, and Jun-Yan Zhu. Semantic image synthesis with spatially-adaptive normalization. In *Proceedings of the IEEE/CVF conference on computer vision and pattern recognition*, pages 2337–2346, 2019. 1, 7
- [58] Jonas Pfeiffer, Aishwarya Kamath, Andreas Rücklé, Kyunghyun Cho, and Iryna Gurevych. Adapterfusion: Non-destructive task composition for transfer learning. *arXiv preprint arXiv:2005.00247*, 2020. 3
- [59] Dustin Podell, Zion English, Kyle Lacey, Andreas Blattmann, Tim Dockhorn, Jonas Müller, Joe Penna, and Robin Rombach. Sdxl: Improving latent diffusion models for high-resolution image synthesis. *arXiv preprint arXiv:2307.01952*, 2023. 1, 7
- [60] Alec Radford, Jong Wook Kim, Chris Hallacy, Aditya Ramesh, Gabriel Goh, Sandhini Agarwal, Girish Sastry, Amanda Askell, Pamela Mishkin, Jack Clark, et al. Learning transferable visual models from natural language supervision. In *International conference on machine learning*, pages 8748–8763. Pmlr, 2021. 1, 3
- [61] Aditya Ramesh, Mikhail Pavlov, Gabriel Goh, Scott Gray, Chelsea Voss, Alec Radford, Mark Chen, and Ilya Sutskever. Zero-shot text-to-image generation. In *International conference on machine learning*, pages 8821–8831. Pmlr, 2021. 7
- [62] Aditya Ramesh, Prafulla Dhariwal, Alex Nichol, Casey Chu, and Mark Chen. Hierarchical text-conditional image generation with clip latents. *arXiv preprint arXiv:2204.06125*, 1(2):3, 2022. 7
- [63] Robin Rombach, Andreas Blattmann, Dominik Lorenz, Patrick Esser, and Björn Ommer. High-resolution image synthesis with latent diffusion models. In *Proceedings of the IEEE/CVF conference on computer vision and pattern recognition*, pages 10684–10695, 2022. 1, 7
- [64] Andreas Rossler, Davide Cozzolino, Luisa Verdoliva, Christian Riess, Justus Thies, and Matthias Nießner. Faceforensics++: Learning to detect manipulated facial images. In *Proceedings of the IEEE/CVF international conference on computer vision*, pages 1–11, 2019. 7
- [65] Axel Sauer, Katja Schwarz, and Andreas Geiger. Stylegan-xl: Scaling stylegan to large diverse datasets. In *ACM SIGGRAPH 2022 conference proceedings*, pages 1–10, 2022. 2, 7
- [66] Kaede Shiohara, Xingchao Yang, and Takafumi Takeuchi. Blendface: Re-designing identity encoders for face-swapping. In *Proceedings of the IEEE/CVF international conference on computer vision*, pages 7634–7644, 2023. 7
- [67] Chuangchuang Tan, Yao Zhao, Shikui Wei, Guanghua Gu, and Yunchao Wei. Learning on gradients: Generalized artifacts representation for gan-generated images detection. In *Proceedings of the IEEE/CVF Conference on Computer Vision and Pattern Recognition*, pages 12105–12114, 2023. 3
- [68] Chuangchuang Tan, Yao Zhao, Shikui Wei, Guanghua Gu, Ping Liu, and Yunchao Wei. Frequency-aware deepfake detection: Improving generalizability through frequency space domain learning. In *Proceedings of the AAAI Conference on Artificial Intelligence*, pages 5052–5060, 2024. 1, 3, 6, 2
- [69] Chuangchuang Tan, Yao Zhao, Shikui Wei, Guanghua Gu, Ping Liu, and Yunchao Wei. Rethinking the up-sampling operations in cnn-based generative network for generalizable deepfake detection. In *Proceedings of the IEEE/CVF Conference on Computer Vision and Pattern Recognition*, pages 28130–28139, 2024. 3, 6, 8, 1, 2
- [70] Chuangchuang Tan, Renshuai Tao, Huan Liu, Guanghua Gu, Baoyuan Wu, Yao Zhao, and Yunchao Wei. C2p-clip: Injecting category common prompt in clip to enhance generalization in deepfake detection. In *Proceedings of the AAAI Conference on Artificial Intelligence*, pages 7184–7192, 2025. 1, 3, 5, 6, 7, 2
- [71] Renshuai Tao, Chuangchuang Tan, Huan Liu, Jiakai Wang, Haotong Qin, Yakun Chang, Wei Wang, Rongrong Ni, and Yao Zhao. Sagnet: Decoupling semantic-agnostic artifacts from limited training data for robust generalization in deepfake detection. *IEEE Transactions on Information Forensics and Security*, 2025. 3
- [72] Midjourney Team. Midjourney v6.1. <https://www.midjourney.com/home>, . 2024. 7
- [73] OpenAI Team. Dall-e 3 ai image generator. <https://dalle3.ai/>, . 2024. 7
- [74] Yonglong Tian, Dilip Krishnan, and Phillip Isola. Contrastive representation distillation. *arXiv preprint arXiv:1910.10699*, 2019. 3
- [75] Haofan Wang, Ashley Kleyhans, and Abe Estrada. Inswap. <https://github.com/haofanwang/inswapper>. 2023. 7
- [76] Qixun Wang, Xu Bai, Haofan Wang, Zekui Qin, Anthony Chen, Huaxia Li, Xu Tang, and Yao Hu. Instantid: Zero-shot identity-preserving generation in seconds. *arXiv preprint arXiv:2401.07519*, 2024. 7
- [77] Sheng-Yu Wang, Oliver Wang, Richard Zhang, Andrew Owens, and Alexei A Efros. Cnn-generated images are surprisingly easy to spot... for now. In *Proceedings of the IEEE/CVF conference on computer vision and pattern recognition*, pages 8695–8704, 2020. 3, 6, 8, 1, 2
- [78] Tao Wang, Li Yuan, Xiaopeng Zhang, and Jiashi Feng. Distilling object detectors with fine-grained feature imitation. In *Proceedings of the IEEE/CVF conference on computer vision and pattern recognition*, pages 4933–4942, 2019. 3
- [79] Zhendong Wang, Jianmin Bao, Wengang Zhou, Weilun Wang, Hezhen Hu, Hong Chen, and Houqiang Li. Dire for diffusion-generated image detection. In *Proceedings of the IEEE/CVF International Conference on Computer Vision*, pages 22445–22455, 2023. 3

- [80] Yixuan Wei, Han Hu, Zhenda Xie, Ze Liu, Zheng Zhang, Yue Cao, Jianmin Bao, Dong Chen, and Baining Guo. Improving clip fine-tuning performance. In *Proceedings of the IEEE/CVF International Conference on Computer Vision*, pages 5439–5449, 2023. 3
- [81] Jevin West and Carl Bergstrom. Which face is real? <https://www.whichfaceisreal.com/>. 2019. 7
- [82] Jiahui Wu, Yu Zhu, Xiaoben Jiang, Yatong Liu, and Jiajun Lin. Local attention and long-distance interaction of rppg for deepfake detection. *The Visual Computer*, 40(2):1083–1094, 2024. 1
- [83] Siyue Wu, Hongzhan Chen, Xiaojun Quan, Qifan Wang, and Rui Wang. Ad-kd: Attribution-driven knowledge distillation for language model compression. *arXiv preprint arXiv:2305.10010*, 2023. 3
- [84] Yi Wu, Ziqiang Li, Heliang Zheng, Chaoyue Wang, and Bin Li. Infinite-id: Identity-preserved personalization via id-antics decoupling paradigm. In *European Conference on Computer Vision*, pages 279–296. Springer, 2024. 1, 2, 7
- [85] Wukong. <https://xihe.mindspore.cn/modelzoo/wukong>. 2022. 7
- [86] Jiazhen Yan, Ziqiang Li, Ziwen He, and Zhangjie Fu. Generalizable deepfake detection via effective local-global feature extraction. *arXiv preprint arXiv:2501.15253*, 2025. 3, 6, 1, 2
- [87] Jiazhen Yan, Fan Wang, Weiwei Jiang, Ziqiang Li, and Zhangjie Fu. Ns-net: Decoupling clip semantic information through null-space for generalizable ai-generated image detection. *arXiv preprint arXiv:2508.01248*, 2025. 3, 5, 6, 7, 8, 1, 2
- [88] Shilin Yan, Ouxiang Li, Jiayin Cai, Yanbin Hao, Xiaolong Jiang, Yao Hu, and Weidi Xie. A sanity check for ai-generated image detection. *arXiv preprint arXiv:2406.19435*, 2024. 6, 8, 1, 2
- [89] Zhiyuan Yan, Jiangming Wang, Peng Jin, Ke-Yue Zhang, Chengchun Liu, Shen Chen, Taiping Yao, Shouhong Ding, Baoyuan Wu, and Li Yuan. Orthogonal subspace decomposition for generalizable ai-generated image detection. *arXiv preprint arXiv:2411.15633*, 2024. 1, 3, 5, 6, 2
- [90] Jing Yang, Brais Martinez, Adrian Bulat, Georgios Tzimiropoulos, et al. Knowledge distillation via softmax regression representation learning. *International Conference on Learning Representations (ICLR)*, 2021. 3
- [91] Yongqi Yang, Zhihao Qian, Ye Zhu, Olga Russakovsky, and Yu Wu. D³: Scaling up deepfake detection by learning from discrepancy. In *Proceedings of the Computer Vision and Pattern Recognition Conference*, pages 23850–23859, 2025. 3
- [92] Hu Ye, Jun Zhang, Sibao Liu, Xiao Han, and Wei Yang. Ip-adapter: Text compatible image prompt adapter for text-to-image diffusion models. *arXiv preprint arXiv:2308.06721*, 2023. 7
- [93] Xiao Yu, Kejiang Chen, Kai Zeng, Han Fang, Zijin Yang, Xiuwei Shang, Yuang Qi, Weiming Zhang, and Nenghai Yu. Semgir: Semantic-guided image regeneration based method for ai-generated image detection and attribution. In *Proceedings of the 32nd ACM International Conference on Multimedia*, pages 8480–8488, 2024. 3
- [94] Maxime Zanella and Ismail Ben Ayed. Low-rank few-shot adaptation of vision-language models. In *Proceedings of the IEEE/CVF Conference on Computer Vision and Pattern Recognition*, pages 1593–1603, 2024. 7
- [95] Bowen Zhang, Shuyang Gu, Bo Zhang, Jianmin Bao, Dong Chen, Fang Wen, Yong Wang, and Baining Guo. Styleswin: Transformer-based gan for high-resolution image generation. In *Proceedings of the IEEE/CVF conference on computer vision and pattern recognition*, pages 11304–11314, 2022. 7
- [96] Haifeng Zhang, Qinghui He, Xiuli Bi, Weisheng Li, Bo Liu, and Bin Xiao. Towards universal ai-generated image detection by variational information bottleneck network. In *Proceedings of the Computer Vision and Pattern Recognition Conference*, pages 23828–23837, 2025. 1, 3, 5
- [97] Hanqing Zhao, Wenbo Zhou, Dongdong Chen, Tianyi Wei, Weiming Zhang, and Nenghai Yu. Multi-attentional deepfake detection. In *Proceedings of the IEEE/CVF conference on computer vision and pattern recognition*, pages 2185–2194, 2021. 1
- [98] Chende Zheng, Chenhao Lin, Zhengyu Zhao, Hang Wang, Xu Guo, Shuai Liu, and Chao Shen. Breaking semantic artifacts for generalized ai-generated image detection. *Advances in Neural Information Processing Systems*, 37:59570–59596, 2024. 3
- [99] Jun-Yan Zhu, Taesung Park, Phillip Isola, and Alexei A Efros. Unpaired image-to-image translation using cycle-consistent adversarial networks. In *Proceedings of the IEEE international conference on computer vision*, pages 2223–2232, 2017. 7
- [100] Mingjian Zhu, Hanting Chen, Qiangyu Yan, Xudong Huang, Guanyu Lin, Wei Li, Zhijun Tu, Hailin Hu, Jie Hu, and Yunhe Wang. Genimage: A million-scale benchmark for detecting ai-generated image. *Advances in Neural Information Processing Systems*, 36, 2024. 6, 7, 8, 2

DGS-Net: Distillation-Guided Gradient Surgery for CLIP Fine-Tuning in AI-Generated Image Detection

Supplementary Material

7. Compared Detectors

To provide a comprehensive benchmark for comparison, we introduce 11 existing state-of-the-art detection methods, including CNN-Spot (CVPR 2020) [77], UnivFD (CVPR 2023) [55], FreqNet (AAAI 2024) [68], NPR (CVPR 2024) [69], Ladeda (arXiv 2024) [2], AIDE (ICLR 2025) [88], C2P-CLIP (AAAI 2025) [70], DFFreq (arXiv 2025) [86], SAFE (KDD 2025) [42], Effort (ICML 2025) [89] and NS-Net (arxiv 2025) [87], details are as follow:

1) CNN-Spot (CVPR 2020) [77]. CNN-Spot employs convolutional neural networks to detect synthetic content by analyzing common spatial artifacts in AI-generated images. It captures hierarchical features directly from pixel data, enabling the detection of generation anomalies.

2) UnivFD (CVPR 2023) [55]. UnivFD demonstrates that CLIP can effectively extract artifacts from images. By training a classifier on these features, it achieves strong cross-generator generalization performance.

3) FreqNet (AAAI 2024) [68]. FreqNet isolates high-frequency components of images via an FFT-based high-pass filter and introduces a frequency-domain learning block. This block transforms intermediate feature maps using FFT, applies learnable magnitude and phase adjustments, and reconstructs them with iFFT, enabling direct optimization in the frequency domain.

4) NPR (CVPR 2024) [69]. NPR targets structural artifacts introduced by up-sampling layers in generative models. It transforms input images into NPR maps that capture signed intensity differences between each pixel and its neighbors, explicitly revealing local dependency patterns characteristic of synthetic up-sampling operations.

5) Ladeda (arxiv 2024) [2]. LaDeDa is a patch-level deepfake detector that partitions each input image into 9×9 pixel patches and processes them using a BagNet-style ResNet-50 variant with its receptive field constrained to the same 9×9 region. The model assigns a deepfake likelihood to each patch, and the final prediction is obtained by globally pooling the patch-level scores.

6) AIDE (ICLR 2025) [88]. AIDE combines low-level patch statistics with high-level semantics for AI-generated image detection. It employs two expert branches: a semantic branch, which leverages CLIP-ConvNeXt embeddings to detect content inconsistencies, and a patchwise branch, which selects patches by spectral energy and applies a lightweight CNN to capture fine-grained artifacts.

7) C2P-CLIP (AAAI 2025) [70]. C2P-CLIP concludes that CLIP achieves classification by matching similar concepts

rather than discerning true and false. Based on this conclusion, they propose category common prompts to fine-tune the image encoder by manually constructing category concepts combined with contrastive learning.

8) DFFreq (arxiv 2025) [86]. DFFreq first utilizes a sliding window to restrict the attention mechanism to a local window, and reconstruct the features within the window to model the relationships between neighboring internal elements within the local region. Then, a dual frequency domain branch framework consisting of four frequency domain subbands of DWT and the phase part of FFT is designed to enrich the extraction of local forgery features from different perspectives.

9) SAFE (KDD 2025) [42]. SAFE replaces conventional resizing with random cropping to better preserve high-frequency details, applies data augmentations such as ColorJitter and RandomRotation to break correlations tied to color and layout, and introduces patch-level random masking to encourage the model to focus on localized regions where synthetic pixel correlations typically emerge.

10) Effort (ICML 2025) [89]. Effort find that a naively trained detector very quickly shortcuts to the seen fake patterns, collapsing the feature space into a low-ranked structure that limits expressivity and generalization. Thus, they decompose the feature space into two orthogonal subspaces, for preserving pre-trained knowledge while learning forgery.

11) NS-Net (arxiv 2025) [87]. NS-Net uses the feature homogeneity extracted by the text encoder to replace the semantic information of the features extracted by the image encoder, and uses NULL-Space to decouple the semantic information, retaining the artifact information related to the forgery detection task.

8. Evaluation on UniversalFakeDetect

Table 7 underscores our method’s capability in detecting unknown Diffusion-based fake images. Specifically, it achieves mean Accuracy (Acc.) and mean Average Precision (A.P.) of 99.0% and 100.0%, respectively. Our method achieves nearly 100% detection accuracy on almost all datasets, with particularly strong performance on the Guided dataset, where it surpasses the best existing method by 5.4%, demonstrating the method’s strong generalization ability.

9. AP Result on AIGIBench

Follow the evaluation metrics used in baselines [55, 68], which include average precision score (A.P.) and accuracy (Acc.), we add the A.P. results on AIGIBench [47], as shown

Detection Method	Guided		Glide_50_27		Glide_100_10		Glide_100_27		LDM_100		LDM_200		LDM_200_cfg		DALLE		Mean	
	Acc.	A.P.	Acc.	A.P.	Acc.	A.P.	Acc.	A.P.	Acc.	A.P.	Acc.	A.P.	Acc.	A.P.	Acc.	A.P.	mAcc.	mA.P.
CNN-Spot [77]	51.3	70.8	52.2	76.9	52.2	78.0	52.4	76.8	60.6	88.7	62.0	90.1	68.0	93.8	51.6	62.7	56.3	79.7
UnivFD [55]	64.2	81.0	84.0	92.5	84.5	92.1	84.3	92.3	82.5	91.4	82.5	91.4	73.4	84.7	69.0	80.3	78.1	88.2
FreqNet [68]	68.2	78.5	89.8	97.8	90.2	97.9	88.8	97.6	97.6	99.7	98.1	99.8	97.3	99.7	70.5	93.1	87.6	95.5
NPR [69]	64.6	83.0	80.9	99.3	80.2	99.0	79.9	99.3	88.0	99.9	86.9	99.9	94.6	100.0	63.6	98.9	79.8	97.4
Ladeda [2]	79.8	87.5	98.3	99.8	98.2	99.8	98.5	99.8	98.6	99.9	98.5	99.9	98.0	99.8	83.9	98.5	94.2	98.1
AIDE [88]	90.1	98.5	98.3	99.9	97.9	99.8	98.1	99.8	98.4	99.9	98.3	100.0	98.5	100.0	96.7	99.5	97.0	99.7
C2P-CLIP* [70]	80.3	98.6	94.3	99.6	93.0	99.8	89.3	99.4	<u>100.0</u>	100.0	100.0	100.0	<u>100.0</u>	100.0	100.0	100.0	94.6	99.7
DFFreq [86]	90.3	99.2	94.8	99.2	95.7	99.2	93.9	99.0	99.3	100.0	99.2	100.0	99.2	100.0	95.2	99.5	96.0	99.5
SAFE [42]	80.7	96.0	94.8	98.5	95.2	98.4	93.2	97.9	97.2	99.9	97.4	99.9	97.1	99.9	94.7	99.1	93.8	98.7
Effort [89]	76.4	98.3	95.7	99.8	95.7	99.8	93.7	99.6	99.9	100.0	<u>100.0</u>	100.0	99.8	100.0	<u>100.0</u>	100.0	95.2	99.7
NS-Net [87]	<u>92.5</u>	<u>99.4</u>	<u>98.2</u>	<u>99.9</u>	<u>99.0</u>	<u>99.9</u>	<u>98.2</u>	<u>99.8</u>	100.0	<u>100.0</u>	100.0	<u>100.0</u>	100.0	<u>100.0</u>	100.0	<u>100.0</u>	<u>98.5</u>	<u>99.9</u>
Ours	97.9	99.8	98.9	99.9	99.9	100.0	98.5	99.9	99.6	100.0	99.7	100.0	99.4	100.0	99.5	100.0	99.0	100.0

Table 7. Cross-Diffusion-Sources Evaluation on the Diffusion Test Set of UniversalFakeDetect [55].

Generator	CNN-Spot	UnivFD	FreqNet	NPR	Ladeda	AIDE	C2P-CLIP*	DFFreq	SAFE	Effort	NS-Net	Ours
ProGAN	99.9	99.9	100.0	100.0	100.0	99.6	100.0	100.0	100.0	100.0	100.0	100.0
R3GAN	52.4	91.2	55.8	61.1	72.6	97.1	91.3	90.6	99.2	98.2	91.3	97.1
StyleGAN3	85.2	84.5	92.4	91.7	96.9	91.4	99.5	98.1	94.7	98.9	99.4	98.3
StyleGAN-XL	50.2	93.3	83.7	75.3	93.1	93.2	98.9	69.5	90.8	97.0	96.1	97.9
StyleSwim	76.2	95.2	91.6	94.9	98.5	89.3	99.6	99.5	96.7	99.1	97.8	99.6
WFIR	65.5	83.0	57.0	65.5	86.9	90.8	99.6	89.0	60.7	100.0	99.4	99.9
BlendFace	73.2	35.2	34.0	34.7	42.1	54.2	48.9	42.3	44.1	66.1	54.4	65.3
E4S	68.7	57.0	34.5	34.4	49.3	44.3	48.3	41.0	45.6	76.9	49.4	56.8
FaceSwap	58.3	52.3	42.9	43.6	40.9	56.3	70.4	64.9	69.6	85.8	62.5	79.0
InSwap	77.5	40.1	41.8	40.7	47.4	54.6	65.6	57.3	62.3	83.1	67.5	83.1
SimSwap	69.7	40.3	41.7	42.7	42.3	62.7	68.5	57.7	59.9	89.7	69.5	86.0
DALLE-3	68.4	76.4	60.2	70.0	59.8	63.1	56.3	48.5	49.5	60.6	42.2	40.5
FLUX1-dev	72.1	79.5	87.0	99.0	98.7	93.4	84.3	98.2	99.0	74.4	94.1	96.8
Midjourney-V6	59.8	61.5	55.9	76.9	86.9	83.0	84.6	94.2	94.5	90.0	90.0	92.8
GLIDE	59.7	80.2	76.5	94.3	95.0	97.7	94.9	97.7	96.1	96.5	96.1	97.3
Imagen3	57.0	79.3	80.2	94.4	97.2	95.2	93.9	84.7	97.0	97.8	95.9	94.6
SD3	72.7	87.2	81.9	97.2	98.7	98.3	97.1	97.0	99.3	97.9	98.9	99.1
SDXL	63.8	88.0	95.0	94.4	98.5	95.7	97.1	99.1	99.4	98.0	98.2	99.1
BLIP	92.8	95.8	99.8	100.0	99.9	99.5	100.0	100.0	100.0	100.0	100.0	100.0
Infinite-ID	49.1	89.6	73.6	80.4	76.9	94.7	84.2	97.4	98.5	85.7	91.8	97.8
PhotoMaker	57.8	72.2	74.2	53.4	90.7	95.6	69.7	99.0	96.9	69.2	67.8	94.4
Instant-ID	79.9	93.5	86.0	79.2	90.4	96.3	84.9	99.9	94.8	87.1	87.7	97.2
IP-Adapter	65.5	87.3	79.4	91.7	94.3	95.4	95.4	98.8	94.8	98.1	96.2	99.0
SocialRF	50.6	55.2	58.1	68.4	68.3	65.0	67.7	66.9	63.5	65.2	74.6	71.1
CommunityAI	56.7	73.7	63.5	62.9	56.3	61.0	53.2	64.2	64.3	64.3	54.0	52.1
Average	67.3	75.7	69.9	73.9	79.3	82.7	82.2	82.2	82.9	<u>87.2</u>	83.0	87.8

Table 8. Cross-model Average Precision (A.P.) Performance on the AIGIBench [47] Dataset.

Components	Real Image	Generative Adversarial Networks							Other		Diffusion Models							mAcc.	
		Pro-GAN	Cycle-GAN	Big-GAN	Style-GAN	Style-GAN2	Gau-GAN	Star-GAN	WFIR	Deep-fake	SDv1.4	SDv1.5	ADM	GLIDE	Mid-journey	Wukong	VQDM		DALLE2
-(Baseline)	99.9	99.9	99.4	99.6	83.1	87.0	80.6	100.0	9.8	39.3	100.0	99.9	52.1	75.2	54.1	98.9	89.7	69.2	79.9
g_{img}^+, g_{text}^+	99.5	99.9	99.7	99.7	79.7	76.0	90.9	100.0	4.8	32.7	100.0	99.9	61.6	85.7	48.8	99.6	93.7	95.8	81.6
g_{img}^-, g_{text}^-	99.5	100.0	100.0	100.0	81.7	92.7	97.6	100.0	24.6	40.6	100.0	99.9	71.0	90.0	59.4	99.7	96.5	96.8	86.1
g_{img}^-, g_{text}^-	98.1	99.9	100.0	100.0	91.2	96.9	99.7	100.0	69.8	85.7	100.0	99.9	86.5	92.1	77.6	99.9	98.6	98.3	94.1
g_{img}^-, g_{text}^- (Ours)	95.3	100.0	100.0	100.0	99.5	99.8	100.0	100.0	84.6	96.7	100.0	99.9	95.2	99.0	88.0	100.0	99.7	99.6	97.6

Table 9. Cross-model Accuracy (Acc.) Performance on the GenImage [100] Dataset. We further experimentally verify the beneficial and harmful components of the gradient.

in Table 8. Furthermore, our method achieves state-of-the-art performance among the baselines in terms of AP, underscoring the superiority of the proposed approach. This indicates

that our method not only excels in overall prediction accuracy but also maintains robust performance across different decision thresholds, thereby demonstrating its effectiveness

in distinguishing between classes.

10. More Confirmatory Studies

As discussed in Sec. 3 and Sec. 4, we define the positive half-space of text gradients as harmful directions that should be suppressed, while the negative half-space of image gradients corresponds to beneficial directions that preserve the prior knowledge of the pre-trained model. To further validate this definition and theoretical reasoning, we conducted an additional experiment in which we directly used text gradients as harmful directions and treated all image gradients as beneficial directions. The results of this experiment are shown in Table 9. These results clearly demonstrate the necessity of categorizing gradients into harmful and beneficial components and treating them separately. For instance, injecting all image gradients as beneficial yields only limited improvements over the baseline, particularly on diffusion models; likewise, removing all text gradients as harmful results in performance substantially below our approach. In contrast, our method selectively projects and removes only the positive half-space of text gradients (harmful semantics) while injecting only the negative half-space of image gradients (beneficial priors). This strategy achieves the highest mAcc of 97.6%, approaching saturation on multi-class GANs and producing the most significant gains on diffusion models, thereby substantially improving cross-generator generalization.